PROCEEDINGS OF SCIENCE

Anatomy of SU(3) flux tubes at finite temperature

Paolo Cea
Dipartimento di Fisica, Università di Bari,
and INFN - Sezione di Bari, I-70126 Bari, Italy
E-mail: paolo.cea@ba.infn.it

Leonardo Cosmai
INFN - Sezione di Bari, I-70126 Bari, Italy
E-mail: leonardo.cosmai@ba.infn.it

Francesca Cuteri*
Dipartimento di Fisica, Università della Calabria,
and INFN - Gruppo collegato di Cosenza, I-87036 Rende, Cosenza, Italy
E-mail: francesca.cuteri@fis.unical.it

Alessandro Papa
Dipartimento di Fisica, Università della Calabria,
and INFN - Gruppo collegato di Cosenza, I-87036 Rende, Cosenza, Italy
E-mail: alessandro.papa@fis.unical.it

An attempt to adapt the study of color flux tubes to the case of finite temperature has been made. The field is measured both through the correlator of two Polyakov loops, one of which connected to a plaquette, and through a connected correlator of Wilson loop and plaquette in the spatial sublattice. Still the profile of the flux tube resembles the transverse field distribution around an isolated vortex in an ordinary superconductor. The temperature dependence of all the parameters characterizing the flux tube is investigated.

The 33rd International Symposium on Lattice Field Theory
14 -18 July 2015
Kobe International Conference Center, Kobe, Japan

*Speaker.

© Copyright owned by the author(s) under the terms of the Creative Commons
Attribution-NonCommercial-NoDerivatives 4.0 International License (CC BY-NC-ND 4.0).

arXiv:1510.08993v1 [hep-lat] 30 Oct 2015

1. Introduction

The color confinement phenomenon accounts for our inability to detect free colored particles, with the QCD spectrum consisting of color-singlet particle states only. Although yet unexplained from first principles, color confinement can be interpreted within a few possible scenarios and lattice QCD studies are relevant in order to verify/disprove the validity of the different options.

It was conceived, by 't Hooft and Mandelstam, that the QCD vacuum could be modeled as a coherent state of color magnetic monopoles, called *dual superconductor*, since the condensation of color magnetic monopoles is thought to be analogous to the formation of Cooper pairs in the BCS theory of superconductivity [1]. A dual superconductor is a superconductor in which the roles of the electric and magnetic fields are exchanged. The analogy is suggested both by the the absence of free colored states, and by the fact that meson resonances lie approximately on Regge trajectories, indicating that a quark-antiquark $q\bar{q}$ pair is connected by a string with a constant string tension, i.e. with an energy that increases linearly with the distance R between the color charges. Correspondingly, in the large-distance regime, the nonperturbative dynamics squeezes the color-field lines, giving rise to flux tubes connecting the two charges. The formation of color flux tubes can be interpreted as the dual analog of the Meissner effect. Lattice QCD allows us to investigate the color confinement phenomenon nonperturbatively and, in this framework, convincing evidences both for the color magnetic monopole condensation, and for the existence of color tubelike structures, have been produced [2]. In previous studies [3] the tubelike distribution of color fields in presence of static quarks has been studied both in the SU(2) and SU(3) pure gauge theory at zero temperature. As a meaningful extension of those studies, the structure of flux tubes in the SU(3) pure gauge theory at nonzero temperature, and across the deconfinement transition temperature T_c, is now investigated. There is a twofold motivation for this study: on one hand, the nonperturbative study of flux tubes at $T \neq 0$ is relevant to clarify the formation of $c\bar{c}$ and $b\bar{b}$ bound states in heavy-ion collisions at high energies; on the other hand, the study of the behavior of flux tubes across T_c allows us to check the validity of the dual superconductor model. For our investigation we have made use of the MILC code, which has been suitably modified by us in order to introduce the relevant observables. The use of the MILC code will allow, in future, simulations for the physically relevant case of full QCD with dynamical quarks.

The color field distribution generated by a $q\bar{q}$ static pair in the vacuum is probed by means of the connected correlators [2]

$$\rho_P^{\mathrm{conn}} = \frac{\left\langle \mathrm{tr}\left(P(x)LU_PL^\dagger\right)\mathrm{tr}P(y)\right\rangle}{\left\langle \mathrm{tr}\left(P(x)\right)\mathrm{tr}\left(P(y)\right)\right\rangle} - \frac{1}{3}\frac{\left\langle \mathrm{tr}\left(P(x)\right)\mathrm{tr}\left(P(y)\right)\mathrm{tr}\left(U_P\right)\right\rangle}{\left\langle \mathrm{tr}\left(P(x)\right)\mathrm{tr}\left(P(y)\right)\right\rangle} \tag{1.1}$$

and

$$\rho_W^{\mathrm{conn}} = \frac{\left\langle \mathrm{tr}\left(WLU_PL^\dagger\right)\right\rangle}{\left\langle \mathrm{tr}(W)\right\rangle} - \frac{1}{N}\frac{\left\langle \mathrm{tr}(U_P)\mathrm{tr}(W)\right\rangle}{\left\langle \mathrm{tr}(W)\right\rangle}\,. \tag{1.2}$$

In both cases, $U_P = U_{\mu\nu}(x)$ is the plaquette in the (μ,ν) plane, and L is the Schwinger line connecting the plaquette, either to the Wilson loop W, or to a Polyakov loop P; N is the number of colors. A schematic representation of the correlators is given in Fig. 1. The use of the connected correlator (1.2) at $T \neq 0$ is limited to the exploration of the chromomagnetic sector. The linearity of ρ_W^{conn} and ρ_P^{conn} in the field, in the SU(3) case, holds up to terms of order a^2 in the lattice spacing.

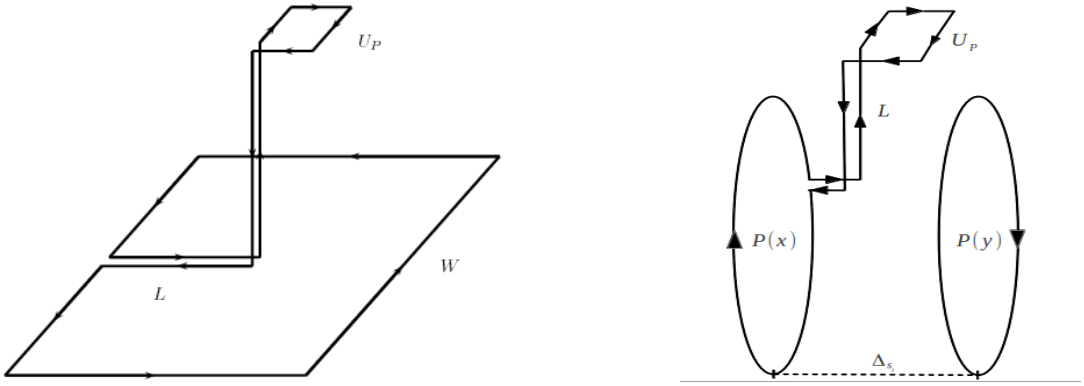

Figure 1: (Left) The connected correlator between the plaquette U_P and the Wilson loop. (Right) The correlator between two Polyakov loops, one of which connected to a plaquette U_P. The subtraction in $\rho^{\text{conn}}_{P,W}$ is not explicitly drawn.

The linear term in $F_{\mu\nu}$, then, dictates the dominant behavior of our correlators in the continuum limit, and a symbolic expression for the naive continuum limit of the connected correlators is

$$\rho^{\text{conn}}_{W,P} \xrightarrow{a\to 0} a^2 g \left[\left\langle n^a F^a_{\mu\nu}\right\rangle_{q\bar{q}}\right], \tag{1.3}$$

In this formula $\langle \quad \rangle_{q\bar{q}}$ denotes the ensemble average of the field projection onto an unknown direction (in color space), n^a, determined by the static $q\bar{q}$ pair, and $\beta = {}^{2N}/_{g^2}$ is the coupling constant. The components of the field strength tensor can, then, be extracted as

$$F^a_{\mu\nu}(x)\, n^a = \sqrt{\frac{\beta}{2N}}\rho^{conn}_{W,P}(x)\ . \tag{1.4}$$

The color field distribution of flux tubes and, in particular, the shape of color fields, in a direction perpendicular to the axis of the flux tube joining the $q\bar{q}$ pair, is probed by varying position and orientation of the plaquette. The dual superconductor model enters our analysis in the choice of the function to fit the transverse shape of the field. Here we exploit the dual analog of a result presented in [4]:

$$E_l(x_t) = \frac{\phi}{2\pi}\frac{\mu^2}{\alpha}\frac{K_0\left[\left(\mu^2 x_t^2+\alpha^2\right)^{1/2}\right]}{K_1[\alpha]} = \frac{\phi}{2\pi}\frac{\mu^2}{\alpha}\frac{K_0[(\mu^2 x_t^2+\alpha^2)^{1/2}]}{K_1[\alpha]}\ , \tag{1.5}$$

where $\mu = {}^1/\lambda$ is the inverse of the London penetration depth, ξ_v is the variational core radius parameter, and the quantity at the left-hand side is the longitudinal chromoelectric field, which has been found (also at $T \neq 0$) to be the only statistically sizable color field component forming the flux tube. By fitting Eq. (1.5) to $E_l(x_t)$ data, one can extract ϕ, λ and ξ_v. The Ginzburg-Landau κ parameter can be obtained by

$$\kappa = \frac{\lambda}{\xi} = \frac{\sqrt{2}}{\alpha}\left[1 - K_0^2(\alpha)/K_1^2(\alpha)\right]^{1/2}\ , \tag{1.6}$$

and the coherence length ξ can be deduced from $\kappa = {}^{\lambda}/_{\xi}$.

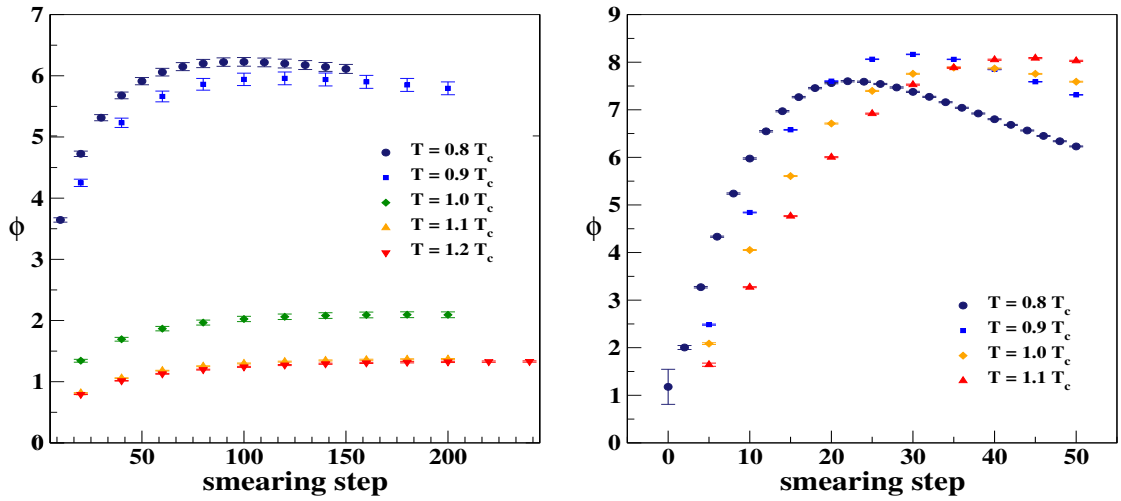

Figure 2: ϕ *vs* smearing for measurements of the Polyakov (left) and Wilson (right) connected correlator at $T \neq 0$, on a $40^3 \times 10$ lattice.

2. Color flux tubes on the lattice

We performed our numerical simulations using the Wilson action on lattices with periodic boundary conditions and the heat-bath algorithm combined with overrelaxation. To reduce the autocorrelation time, measurements were taken every 10 updatings. The considered lattice sizes had temporal extensions ranging from $L_t = 10$ up to $L_t = 16$ and spatial size L_s fixed to keep the aspect ratio equal to four. The temperature varies according to:

$$T = \frac{1}{a(\beta)\, L_t}\,, \tag{2.1}$$

where the scale is fixed with the parameterization in [5] and $\sqrt{\sigma} = 420\,\mathrm{MeV}$. A relevant variable to be taken under control in our simulations is the distance Δ between the static sources (size of the Wilson loop or distance between Polyakov loops). Consistently with our previous studies [3], we have found that Δ has to be chosen in a way that the distance in physical units is beyond half a fermi. In such a distance regime, the only parameter affected by changes in the physical distance, produced for example by keeping Δ fixed in lattice units, while varying β, is ϕ. It was then decided to approximately fix the physical, rather than the lattice, distance between the sources. The advantages are that less statistics is needed for smaller couplings and that the achievement of the continuum limit can be shown already at the level of the measured field. In order to reduce the ultraviolet noise, we applied one step of HYP smearing [6] to links in the temporal direction, with smearing parameters $(\alpha_1, \alpha_2, \alpha_3) = (1.0, 0.5, 0.5)$, and N_{APE} steps of APE smearing [7] to spatial links, with smearing parameter $\alpha_{\mathrm{APE}} = 0.50$. As a criterion to determine the optimal smearing step, the position of the peak in ϕ (signalling the maximal disentanglement of our signal from background noise) has been used.

3. Flux tubes across the deconfinement transition

In this section we present numerical results on the chromoelectric field distribution generated

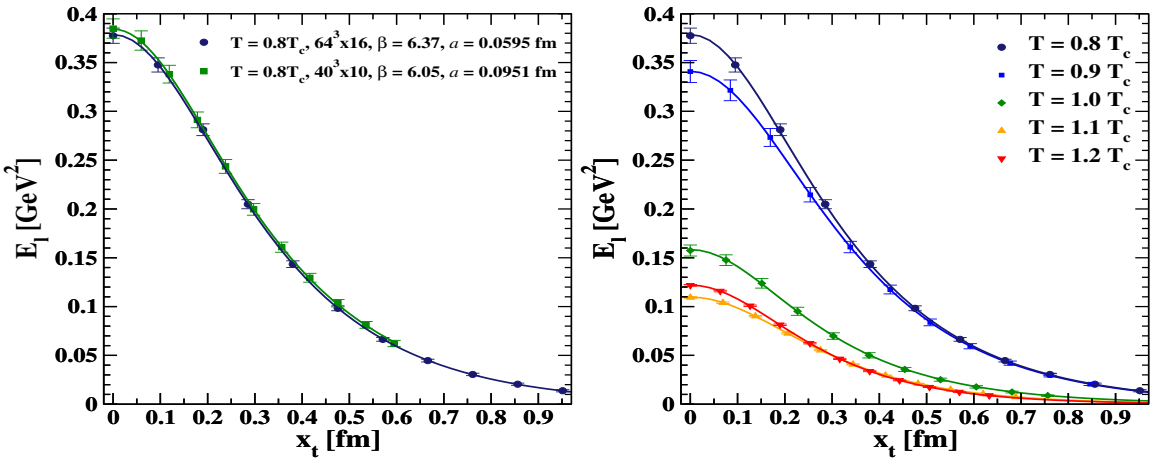

Figure 3: (Left) Scaling of $E_l(x_t)$ at $T \simeq 0.8T_c$. (Right) $E_l(x_t)$ at fixed lattice size $40^3 \times 10$, and couplings $\beta = 6.050, 6.125, 6.200, 6.265, 6.325$ corresponding to temperatures $T/T_c = 0.8, 0.9, 1.0, 1.1, 1.2$. For the critical temperature, we used $T_c = 260\,\text{MeV}$. The solid lines are the fit of our data to Eq. (1.5).

Table 1: Fit values on a $N_s \times N_t = 40^3 \times 10$ lattice for several values of T.

β	Δ [fm]	T/T_c	ϕ	μ	ξ_v	χ^2_r
6.050	0.761	0.8	6.201(68)	0.382(13)	3.117(191)	0.02
6.125	0.761	0.9	5.941(101)	0.337(20)	3.652(360)	0.01
6.200	0.756	1.0	2.061(45)	0.328(22)	3.312(389)	0.01
6.265	0.757	1.1	1.359(9)	0.344(7)	4.286(131)	0.06
6.325	0.760	1.2	1.324(11)	0.332(8)	4.248(142)	0.06

by a static $q\bar{q}$ pair at $T \neq 0$, measured through the connected correlator in Eq. (1.1). Before studying the temperature dependence of the chromoelectric field shape, a scaling analysis was performed at a fixed temperature of $T = 0.8T_c$. As shown in Fig. 3 (Left), $E_l(x_t)$, measured at the optimal smearing step, on lattices with different sizes and at β values tuned in a way to keep the temperature fixed, exhibits the same behavior, thus indicating continuum scaling. Afterwards, the lattice size was fixed to $40^3 \times 10$ and, by varying the coupling β in the range $[6.050 - 6.325]$, the effect on the flux tube of a growing temperature was studied. The results of our analysis are shown in Fig. 3 (Right). To check to what extent the dual superconductor scenario is confirmed by our numerical results, the behavior *vs* temperature of London penetration depth and coherence length was analyzed. Results are shown in Fig. 4. We observe that, while the intensity of the measured chromoelectric field has a substantial drop at T_c, the penetration length λ decreases monotonically across the transition (but from bigger values than what we observed at $T = 0$), while ξ stays approximately constant (even though at a much smaller value than at $T = 0$). According to our numerical findings, flux tubes are somehow "evaporating" in a way that is not consistent with the dual superconductor analogy. In ordinary superconductivity, indeed, both λ and ξ diverge while T_c is approached. Nevertheless, flux tubes do survive across the deconfinement transition temperature and the field shape is well

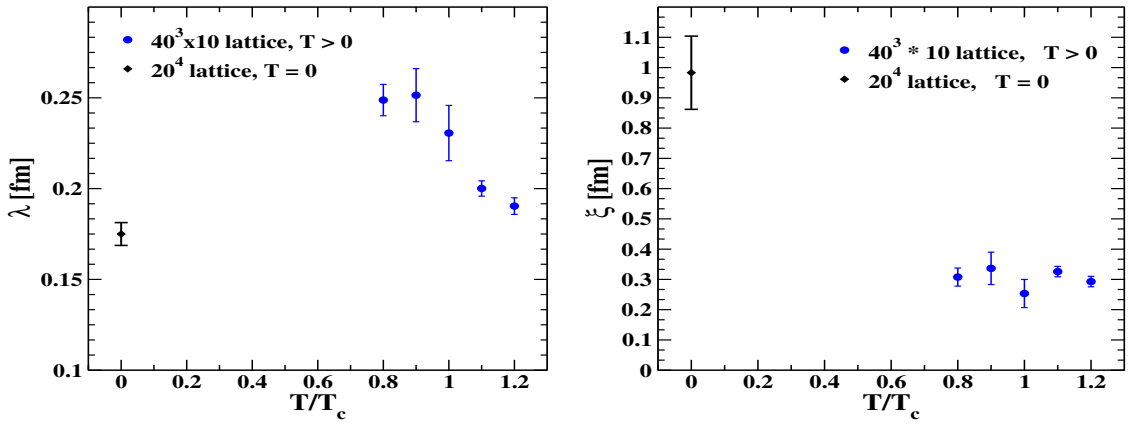

Figure 4: (Left) London penetration depth λ *vs* T/T_c (the $\lambda_{T=0} = 0.1750(63)$ value is included). (Right) Coherence length ξ *vs* T/T_c (the $\xi_{T=0} = 0.983(121)$ value is included).

fitted by the ansatz derived within the dual superconductivity picture, even beyond T_c.

4. Flux tubes across the deconfinement transition in the magnetic sector

In the high-temperature regime, through dimensional reduction, QCD can be reformulated as an effective three-dimensional theory with the scale of the effective couplings given in terms of the temperature [8]. However, straightforward perturbation theory fails in the effective theory, even at high-T, due to the presence of infrared nonperturbative effects which manifest themselves in correlation functions for the spatial components of gauge fields. It is, indeed, known that the spatial Wilson loops obey an area law behavior, with spatial string tension σ_s, also in the high-T phase [9]. An analysis of the temperature dependence of σ_s thus yields information on the importance of the nonstatic sector for long-distance properties of high-T QCD. For $T \geq 2T_c$ the spatial string tension satisfies:

$$\sqrt{\sigma_s} \;=\; \gamma\, g(T)\, T\;, \tag{4.1}$$

where $g(T)$ is the temperature dependent coupling constant, running according to the two-loop β-function, and γ is a constant; $\gamma = 0.586 \pm 0.045$ for SU(3) [9]. In view of this, and for a better understanding of the nonperturbative structure of QCD at high-T, a quantitative description of the properties of the spatial string tension is needed and the study of the Wilson connected correlator, lying in the spatial sublattice, at nonzero temperature provides us with an indirect measurement of σ_s. Our results for the longitudinal chromomagnetic field *vs* x_t are shown in Fig. 5 and the evidence is that our data are well fitted by Eq. (1.5) at all temperatures and the field shape changes with T in a way consistent with a growing spatial string.

Acknowledgments

This work was in part based on the MILC collaboration's public lattice gauge theory code. See `http://physics.utah.edu/~detar/milc.html` and has been partially supported by the INFN - SUMA project. Simulations have been performed on BlueGene/Q at CINECA (CINECA - INFN agreement)

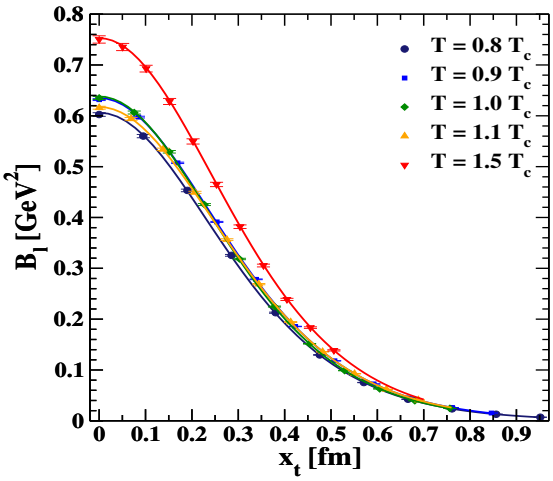

Figure 5: $B_l\,(x_t)$ across the deconfinement transition, as determined from $\rho_W^{\rm conn}$ built in the spatial sublattice. The solid lines are the fit of our data to Eq. (1.5).

References

[1] G. 't Hooft, EPS International Conference (1975); S. Mandelstam, Phys. Rept. **23** (1976) 245; G. Ripka, Lecture notes in physics 639 (2003).

[2] M. Bander, Phys. Rept. **75** (1981) 205; M. Fukugita and T. Niuya, Phys. Lett. B **132** (1983) 374; J. E. Kiskis and K. Sparks, Phys. Rev. D **30** (1984) 1326; J. W. Flower and S. W. Otto, Phys. Lett. B **160** (1985) 128; J. Wosiek and R. W. Haymaker, Phys. Rev. D **36** (1987) 3297; A. Di Giacomo, M. Maggiore and S. Olejnik, Phys. Lett. B **236** (1990) 199; A. Di Giacomo, M. Maggiore and S. Olejnik, Nucl. Phys. B **347** (1990) 441; P. Cea and L. Cosmai, Nuovo Cim. A **107** (1994) 541; P. Cea and L. Cosmai, Nucl. Phys. Proc. Suppl. **34** (1994) 219; V. Singh, D. A. Browne and R. W. Haymaker, Phys. Lett. B **306** (1993) 115; P. Cea and L. Cosmai, Phys. Lett. B **349** (1995) 343; H. Shiba and T. Suzuki, Phys. Lett. B **351** (1995) 519; G. S. Bali, K. Schilling and C. Schlichter, Phys. Rev. D **51** (1995) 5165; N. Arasaki, S. Ejiri, S. i. Kitahara, Y. Matsubara and T. Suzuki, Phys. Lett. B **395** (1997) 275; D. S. Kuzmenko and Y. A. Simonov, Phys. Lett. B **494** (2000) 81; A. Di Giacomo, H. G. Dosch, V. I. Shevchenko and Y. A. Simonov, Phys. Rept. **372** (2002) 319; P. Cea and L. Cosmai, Phys. Rev. D **62** (2000) 094510; P. Cea and L. Cosmai, JHEP **0111** (2001) 064; A. Di Giacomo, B. Lucini, L. Montesi and G. Paffuti, Phys. Rev. D **61** (2000) 034504; J. M. Carmona, M. D'Elia, A. Di Giacomo, B. Lucini and G. Paffuti, Phys. Rev. D **64** (2001) 114507; J. Greensite, Prog. Part. Nucl. Phys. **51** (2003) 1; P. Cea, L. Cosmai and M. D'Elia, JHEP **0402** (2004) 018; A. D'Alessandro, M. D'Elia and E. V. Shuryak, Phys. Rev. D **81** (2010) 094501; R. W. Haymaker and T. Matsuki, Phys. Rev. D **75** (2007) 014501; A. D'Alessandro, M. D'Elia and L. Tagliacozzo, Nucl. Phys. B **774** (2007) 168.

[3] P. Cea and L. Cosmai, Phys. Rev. D **52** (1995) 5152; M. S. Cardaci, P. Cea, L. Cosmai, R. Falcone and A. Papa, Phys. Rev. D **83** (2011) 014502; P. Cea, L. Cosmai and A. Papa, Phys. Rev. D **86** (2012) 054501; P. Cea, L. Cosmai, F. Cuteri and A. Papa, Phys. Rev. D **89** (2014) 094505.

[4] J. R. Clem, J. Low Temp. Phys. **18** (1975) 427.

[5] R. G. Edwards, U. M. Heller and T. R. Klassen, Nucl. Phys. B **517** (1998) 377.

[6] A. Hasenfratz and F. Knechtli, Phys. Rev. D **64** (2001) 034504.

[7] M. Albanese *et al.* [APE Collaboration], Phys. Lett. B **192** (1987) 163.

[8] O. K. Kalashnikov, Fortsch. Phys. **32** (1984) 525; A. Nieto, Int. J. Mod. Phys. A **12** (1997) 1431.

[9] G. S. Bali, J. Fingberg, U. M. Heller, F. Karsch and K. Schilling, Phys. Rev. Lett. **71** (1993) 3059; F. Karsch, E. Laermann and M. Lutgemeier, Phys. Lett. B **346** (1995) 94.